# SSFP and GRE Phase Contrast Imaging Using a Three-Echo Readout

Jon-Fredrik Nielsen* and Krishna S. Nayak

**A technique for rapid in-plane phase-contrast imaging with high signal-to-noise ratio (SNR) is described. Velocity-encoding is achieved by oscillating the readout gradient, such that each 2DFT phase-encode is acquired three times following a single RF slice-selective excitation. Three images are reconstructed, from which both flow velocity and local resonance offset are calculated. This technique is compatible with both gradient-recalled echo (GRE) and balanced steady-state free precession (SSFP) imaging using a single steady-state. The proposed technique enables 1D velocity mapping with 40% higher temporal resolution and 80% higher SNR, compared to conventional PC-MRI using bipolar velocity-encoding gradient pulses. Magn Reson Med 58:1288–1293, 2007. © 2007 Wiley-Liss, Inc.**

**Key words: phase contrast; steady-state free precession; flow quantitation; velocity mapping; field mapping**

## INTRODUCTION

Phase-contrast (PC) MRI (1,2) produces accurate in-vivo measurements of blood flow velocities. Conventional PC-MRI data acquisition is time-consuming, since (1) the acquisition of at least one additional image is required, and (2) the signal-to-noise ratio (SNR) of conventional gradient-recalled echo (GRE) PC-MRI sequences is low, which limits the parallel imaging acceleration factor that can be achieved without compromising the diagnostic value of the PC images.

Balanced steady-state free precession (SSFP) can provide PC measurements with increased SNR (3–5), which can be traded off for reduced acquisition times by means of parallel imaging techniques (6,7). Early approaches to PC-MRI using SSFP require two separate steady-states to be established: one for each value of the gradient first moment (3–5). Interleaving the two image acquisitions is generally not possible in SSFP, due to eddy-current-induced differences in precession. This produces PC measurement errors in regions where the two images are not in perfect spatial alignment, and requires careful and potentially time-consuming switching between the two steady-states. Recently, a new approach to PC-SSFP imaging was proposed (8), in which the readout gradient is oscillated such that each phase-encode is acquired multiple times following a single RF excitation. A train of $N$ echoes is thus acquired, and a PC map is generated from each echo pair, resulting in $N - 1$ PC maps. This approach implicitly assumes that phase-accrual between echoes due to local resonance offset is negligible compared to the velocity-induced phase-accrual, a condition which may be difficult to meet in general.

We introduce a 2DFT PC imaging method that achieves rapid in-plane velocity mapping by oscillating the readout (G$x$) gradient, such that each phase-encode is acquired three times (9,10). From the resulting three echoes, three images are reconstructed, which are used to generate PC measurements that are independent of local resonance offset. We demonstrate that GRE imaging with a three-echo readout allows 1D velocity mapping with nearly twice the temporal resolution compared to a conventional PC-MRI sequence. In addition, we demonstrate that the sequence repetition time (TR) can be sufficiently short to be used with fully balanced SSFP imaging, which allows PC imaging with nearly twice the PC SNR of conventional PC sequences. Three-echo SSFP generates PC from a single steady-state, which virtually eliminates coregistration errors.

## THEORY

Figure 1b shows the proposed three-echo pulse sequence for PC imaging. Velocity-encoding is achieved by oscillating the readout gradient (G$x$) such that each phase-encode line is scanned three times following a single RF excitation. Rather than using a separate bipolar velocity-encoding waveform as is done in conventional PC-MRI (illustrated in Fig. 1a), the readout gradient itself is used to obtain PC. In Fig. 1b, three echoes are formed, from which three images A, B, and C are reconstructed. The phase in each of these images is given by

$$\angle A = \phi_v(\mathrm{TE1}) + \phi_{\mathrm{off}}(\mathrm{TE1}) + \phi_{\mathrm{sys}} \quad [1]$$

$$\angle B = \phi_v(\mathrm{TE2}) + \phi_{\mathrm{off}}(\mathrm{TE2}) + \phi_{\mathrm{sys}} \quad [2]$$

$$\angle C = \phi_v(\mathrm{TE3}) + \phi_{\mathrm{off}}(\mathrm{TE3}) + \phi_{\mathrm{sys}} \quad [3]$$

where $\phi_{\mathrm{off}}(t)$ represents phase accrual due to resonance offset, $\phi_v(t) = \gamma \times m_1(t) \times v$ is the velocity-induced phase, and $\phi_{\mathrm{sys}}$ represents system-related (i.e. object-independent) sources of image phase, such as complex receiver coil sensitivity and gradient/acquisition (DAQ) timing errors. $m_1(t)$ is the gradient first moment at time $t$, with the time-origin $t = 0$ defined as the time of the RF excitation. $\gamma$ is the gyromagnetic ratio.

Magnetic Resonance Engineering Laboratory, Ming Hsieh Department of Electrical Engineering, University of Southern California, Los Angeles, California

Grant sponsor: National Institutes of Health; Grant numbers: R01-HL074332, R21-HL079987

Grant sponsor: American Heart Association; Grant numbers: SDG-0435249N, POST-0625253Y

Grant sponsor: GE Healthcare

*Correspondence to: Jon-Fredrik Nielsen, Ming Hsieh Department of Electrical Engineering, University of Southern California, 3740 McClintock Ave, EEB400, Los Angeles, CA 90089-2564. E-mail: jfnielse@usc.edu

Received 1 September 2006; revised 27 March 2007; accepted 29 March 2007.

DOI 10.1002/mrm.21276

Published online 29 October 2007 in Wiley InterScience (www.interscience.wiley.com).

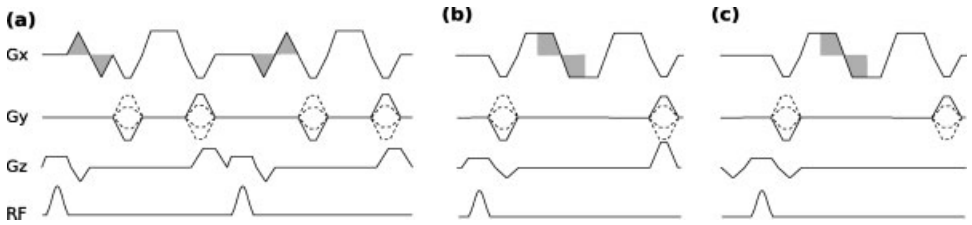


FIG. 1. Pulse sequence diagrams for **(a)** conventional gradient echo phase-contrast pulse sequence with bipolar velocity-encoding gradients, **(b)** the proposed three-echo GRE sequence, and **(c)** the proposed three-echo balanced SSFP sequence. In each sequence diagram, the shaded regions indicate the gradient area used for velocity-encoding.

If we assume that both the spin resonance offset $\omega_{\text{off}}$ and velocity $v$ are constant during data acquisition, we have

$$\phi_{\text{off}}(t) = \omega_{\text{off}} \times t \quad [4]$$

$$\phi_v(\text{TE1}) = \phi_v(\text{TE3}) \quad [5]$$

From Eqs. [1]–[5], we obtain the following expression for the velocity-induced phase contrast:

$$\begin{aligned}\Delta\Phi_v &= \frac{1}{2}\angle(A \times B^*) + \frac{1}{2}\angle(C \times B^*) \\ &= \gamma \times [m_1(\text{TE1}) - m_1(\text{TE2})] \times v \end{aligned} \quad [6]$$

or

$$v = \frac{\angle(A \times B^*) + \angle(C \times B^*)}{2\gamma[m_1(\text{TE1}) - m_1(\text{TE2})]}, \quad [7]$$

where $m_1(t)$ is the first moment of the readout (logical $x$) gradient at time $t$. Note that the measured velocity $v$ depends only on the difference $m_1(\text{TE1}) - m_1(\text{TE2})$ in the gradient first moment between the time-points $t = \text{TE1}$ and $t = \text{TE2}$. In other words, $v$ is independent of the *absolute* value of the first moment at the echo times, which are functions of the entire gradient history following the RF excitation.

Figure 1b shows the proposed three-echo readout implemented as part of a gradient- and RF-spoiled GRE sequence. In this case, a $z$-gradient crusher is applied at the end of the TR, which spoils any transverse magnetization remaining after data acquisition. Compared to conventional PC imaging (Fig. 1a), three-echo GRE PC imaging can be performed in about 40% less time.

Figure 1c shows the proposed three-echo readout as part of a balanced SSFP PC sequence. In Fig. 1c, the 0th moment of all gradients ($x$, $y$, and $z$) are nulled at the end of the sequence. In addition, the $x$- and $z$-gradients are first-moment nulled.

### System-Related Phase-Contrast Offsets

Conventional bipolar PC sequences typically produce unwanted linear and/or DC background PC offsets across the image. Such "phase shading" is due to different residual eddy-current magnetic fields arising in response to the two different bipolar gradient pulses (11). Phase shading is typically either ignored, or estimated from regions in the image that are assumed to be stationary, such as the chest wall.

Three-echo PC-MRI measurements may be influenced by both gradient/acquisition timing delays, and eddy-current-induced magnetic fields. A timing error between the physical gradients and the data acquisition window will result in echo misalignment between echo $B$, and echoes $A$ and $C$, which will produce PC offsets that vary linearly across the image along the readout direction. Furthermore, since the order and timing of gradient ramps are different for three-echo and conventional PC-MRI, eddy-current-induced phase-contrast offsets for these two sequences will in general have different magnitude and/or spatial characteristics.

## METHODS

All experiments were performed on a Signa Excite HD 3T scanner (GE Healthcare, Waukesha, WI) with maximum gradient amplitude and slew rate of 40 mT/m and 150 T/m/s, respectively. Linear shim correction was performed over a 3D volume using the built-in (vendor-provided) shimming tool. Three different imaging sequences were implemented and used in this study: Conventional interleaved 2DFT PC-MRI (Fig. 1a); three-echo GRE PC-MRI (Fig. 1b); and three-echo SSFP PC-MRI (Fig. 1c). All data were acquired with a 20 cm field-of-view (FOV) and a velocity-encoding (VENC) value of 150 cm/s, which corresponds to typical maximum blood flow velocities in the heart in healthy humans. All sequences were designed for 1 mm spatial resolution along the readout direction. Identical readout gradient waveforms (and hence the same VENC) were used for phantom and in-vivo (both cardiac and carotid) measurements. The TR was 4.3, 5.4, and 5.4 ms for the conventional PC, three-echo GRE, and three-echo SSFP sequences, respectively. The conventional and three-echo GRE sequences used RF-spoiling. For the three-echo SSFP sequence, the RF phase was incremented by 180° every TR ($\alpha, -\alpha$ phase cycling). To preserve the steady-state, sequences were executed continuously during image acquisition. Prior to acquiring the first phase-encode line, the sequence was repeated 100 times to allow sufficient time for the magnetization to reach a steady-state (12). Data were sampled on the gradient ramps (in order to reduce TR), which causes nonuniform $k$-space sampling at high spatial frequencies. The data were therefore resampled (gridded) onto an equidistant Cartesian grid prior to inverse Fourier transforming. PC images were generated using the multiple-coil reconstruction proposed by Bernstein et al. (13). All data processing were performed in Matlab (Mathworks, South Natick, MA).

### Stationary Phantom Measurements

To characterize PC offsets due to eddy-currents and gradient/acquisition timing errors, PC data were obtained in a stationary uniform cylindrical phantom of diameter 16 cm containing distilled water doped with a T1 shortening agent (measured T1 = 170 ms), using a birdcage transmit-receive headcoil. The voxel size was $1 \times 1 \times 7$ mm$^3$, and the RF flip angle was 25° for all sequences. Gradient shims were adjusted to introduce approximately linear resonance offset variation across the uniform phantom. This was done to determine whether the three-echo PC estimate is in fact independent of phase-accrual due to local variations in resonance offsets.

### In-Vivo Velocity Measurements

In-vivo measurements were performed for the purpose of (1) determining whether in-vivo three-echo PC-MRI measurements are in quantitative agreement with those obtained using a conventional PC-MRI sequence, and (2) demonstrating the feasibility of using three-echo PC-MRI for high-resolution cardiac flow imaging with increased temporal resolution and SNR, compared to conventional PC-MRI.

To determine the accuracy of three-echo PC-MRI with respect to the use of conventional bipolar flow-encoding gradients, measurements of the carotid arteries were obtained in one healthy volunteer, using a four-channel carotid receive coil. The carotids were chosen because they exhibit little or no respiratory motion, and can be imaged during free breathing. Images were acquired in the plane of the carotid bifurcation, with the readout direction oriented along the length of the common carotid artery. Imaging parameters were chosen to ensure high temporal resolution within a relatively short scan time, such that (1) rapid changes in blood flow velocity could be tracked by both methods (e.g. peak flow is not underestimated due to insufficient temporal resolution), and (2) multiple (10) repetitions of each acquisition could be performed during the same scan session, in order to produce estimates of measurement uncertainty (e.g. stemming from physiological variability). Carotid measurements were prospectively ECG-gated CINE acquisitions with $1 \times 4 \times 10$ mm$^2$ voxel size and a flip angle of 20°, obtained during free breathing. Fifty phase-encode lines were acquired during 25 R-R intervals (two views per cardiac phase), resulting in a temporal resolution of 17.2 ms and 10.7 ms for the bipolar and three-echo PC-MRI acquisitions, respectively.

To demonstrate the use of three-echo PC-MRI for high-resolution cardiac flow imaging with increased temporal resolution and SNR, in-vivo cardiac velocity measurements were obtained in two healthy volunteers, using an eight-channel cardiac receive coil. Images were acquired in a three-chamber view, with the readout direction oriented along the left ventricular outflow tract (LVOT). All in-vivo cardiac acquisitions were prospectively ECG-gated CINE acquisitions with $1 \times 1 \times 7$ mm$^3$ voxel size and a flip angle of 25°, obtained during a single breath-hold. Two-hundred phase-encode lines were acquired during 25 R-R intervals (eight views per cardiac phase), resulting in a temporal resolution of 70 ms and 43 ms for the bipolar and three-echo acquisitions, respectively. The phase SNR was measured in multiple-pixel regions-of-interest (ROI) inside the blood and LV myocardium, by dividing the mean signal inside the ROI by the standard deviation of the PC values within the ROI.

## RESULTS

### Stationary Phantom Results

Figure 2 shows PC images acquired in a uniform static phantom, using both a conventional bipolar PC sequence (a–c), and the proposed three-echo SSFP PC sequence (d–f). Figure 2a shows the PC map obtained with a conventional bipolar GRE-PC readout. Although not apparent in the image in (a), the measured PC values vary linearly along the readout direction (vertical). Figure 2b shows the PC map after correcting for DC and linear phase along the readout

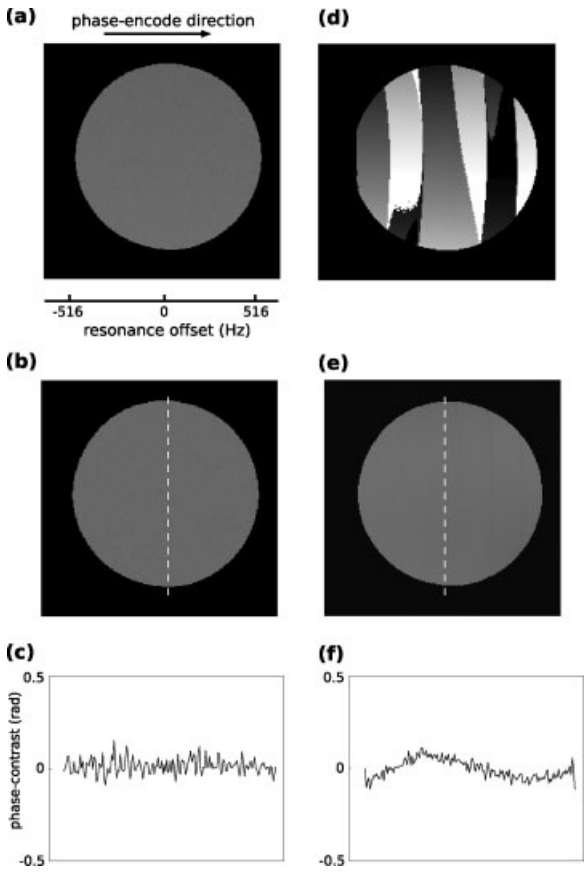


FIG. 2. Phase-contrast maps of a uniform water-filled stationary phantom. Gradient shims were adjusted to generate approximately linear resonance offset variation along the phase-encode direction (horizontal in the images). **(a)** Uncorrected phase-contrast map obtained with a conventional bipolar GRE-PC readout. Although not apparent in this image, "phase shading" is present along the readout direction (vertically in the images). **(b)** Phase-contrast map after DC and linear phase correction along the readout direction. **(c)** PC values along the dotted line in **(b)**. **(d)** Uncorrected phase-contrast map obtained with the proposed three-echo SSFP technique. Phase-shading is apparent along the readout direction. **(e)** Phase-contrast map after correcting for phase-shading and phase-wrapping. **(f)** PC values along the dotted line in **(e)**.

direction. Plotting the PC values along the dotted line in (b) produces the curve in (c).

Figure 2d shows the PC values obtained using the three-echo SSFP technique. In this acquisition, the phase shading was more significant than in (a), which indicates that a small (less than 4 μs) timing error exists between the data acquisition window and the physical gradients. In addition, since three different echo times are used to calculate PC values, phase-wrapping occurs for sufficiently large resonance offset values. Phase-wrapping, combined with a linear background phase, produces the pattern of skewed alternating light and dark patches in the uncorrected phase image in Fig. 2d. Applying DC and linear phase correction (as described in the Methods section) and phase-unwrapping produces the PC image in Fig. 2e. Plotting the PC values along the dotted line produces the curve in Fig. 2f, which shows that some (maximum deviation of less than ±0.1 rad from 0) nonlinear background phase remains after DC and linear phase correction. The PC values along the phase-encode direction are nearly constant in the corrected image (not shown), which indicates that the intentionally introduced spatially varying resonance offsets have been properly accounted for in the three-echo PC reconstruction.

### In-Vivo Results

Figure 3 shows time–velocity curves inside the common carotid artery in a healthy volunteer obtained using both conventional PC-MRI (dashed curve) and three-echo GRE PC-MRI (solid curve). Each acquisition was repeated 10 times, and the curves show the mean value for each technique. The error bars show the measurement variability, and equals ± one standard deviation calculated from the 10 repetitions of each imaging sequence. There is good agreement between the solid and dashed curve, indicating that conventional and three-echo PC-MRI produce comparable velocity measurements, in spite of the different velocity-encoding schemes used.

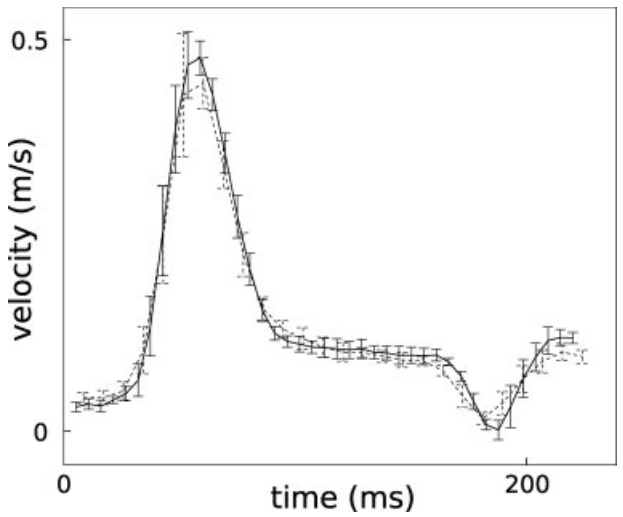


FIG. 3. Time–velocity curves in the common carotid artery in a healthy volunteer, obtained using both conventional PC-MRI (dashed curve) and three-echo GRE PC-MRI (solid curve). Each sequence was repeated 10 times, and the curves and error bars indicate the mean and standard deviation from these measurements. There is good agreement between the solid and dashed curves, indicating that conventional and three-echo PC-MRI produce comparable velocity measurements, in spite of the different velocity-encoding schemes used.

In-vivo cardiac results (three-chamber view) from a healthy volunteer are shown in Fig. 4. Figures 4a–c shows gray-scale PC images of the LVOT in systole, acquired using (a) conventional PC-MRI, (b) three-echo GRE PC-MRI, and (c) three-echo SSFP PC-MRI. Figures 4d–f shows the same PC data as in Figures 4a–c, but displays the data in 3D. In Fig. 4d–f, the PC value in each pixel was used to encode both the height and the color of that pixel. In all images in Fig. 4, the presence of fast blood flow through the aorta is evident. However, the improved SNR in the three-echo acquisitions is evident upon visual inspection of these images. Quantitative measurements in two volunteers show a mean 172 and 198% SNR increase in blood and myocardium, respectively, using three-echo SSFP PC-MRI, compared to a conventional PC-MRI acquisition.

## DISCUSSION

In this work, DC and linear phase offsets were either adjusted based on known stationary regions in the image, or estimated from quiescent portions of the time–velocity curves. Alternatively, it is possible to adapt phase-correction techniques developed for echo-planar imaging (14,15). These techniques are not restricted to linear correction, and can be used to correct residual nonlinear PC offsets, such as those observed in Fig. 2f.

For cardiac SSFP imaging at 3T, a TR of less than 4 ms is desirable (16), which would exclude the use of three-echo SSFP PC-MRI at this field strength. To overcome this, three-echo SSFP PC-MRI may be implemented as a Wideband SSFP sequence (17), which uses alternating TR values to enable the use of a TR greater than the reciprocal of the necessary bandwidth.

In three-echo PC-MRI, the FOV and the spatial resolution along the readout direction place an upper bound on the VENC value. For example, for a 30 cm FOV, 1.5 mm in-plane spatial resolution, and using ramp sampling, the maximum possible VENC is 4.7 m/s. Lower VENCs can be achieved by adjusting the readout gradient plateau widths (and hence the spatial resolution along the readout direction) for each of the three echoes, with a subsequent increase in TR. Figure 5 illustrates the range of spatial resolutions and VENCs that are possible for a given TR.

The phase-encode FOV can be set independently of the readout FOV and spatial resolution (which determine the VENC), since the readout low-pass filter suppresses signal from outside the readout FOV. This is important for applications such as cardiac imaging using parallel imaging, which may require a phase-encode FOV that covers the full width of the torso (18) (typically 30–40 cm).

Although the SNR benefit of SSFP PC-MRI vs. GRE-based measurements has been established (3,4), the absolute SNR

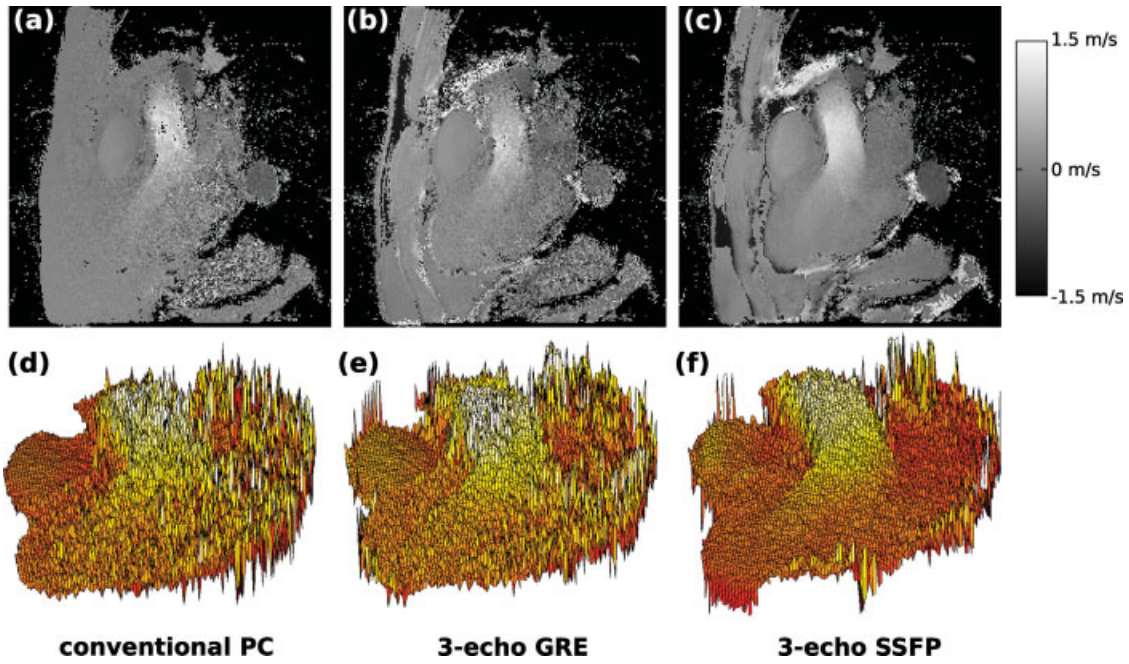


FIG. 4. Phase-contrast maps of the left ventricular outflow tract (LVOT) in systole obtained using (**a** and **d**) a conventional PC sequence with bipolar velocity-encoding gradients, (**b** and **e**) the proposed three-echo GRE sequence, and (**c** and **f**) the proposed three-echo SSFP sequence. The velocity-encoding direction is vertical in the images. The grayscale images (**a**–**c**) were thresholded based on the pixel intensity values in the three-echo SSFP magnitude image (not shown). Note that these images have high spatial resolution, which results in a relatively low SNR compared to measurements obtained with typical clinical phase-contrast protocols.

increase (in %) is expected to vary with the degree of partial saturation, and the imaging flip angle. For example, in regions of rapid through-plane flow, the relative advantage of SSFP PC-MRI may decrease with increasing GRE imaging flip angle.

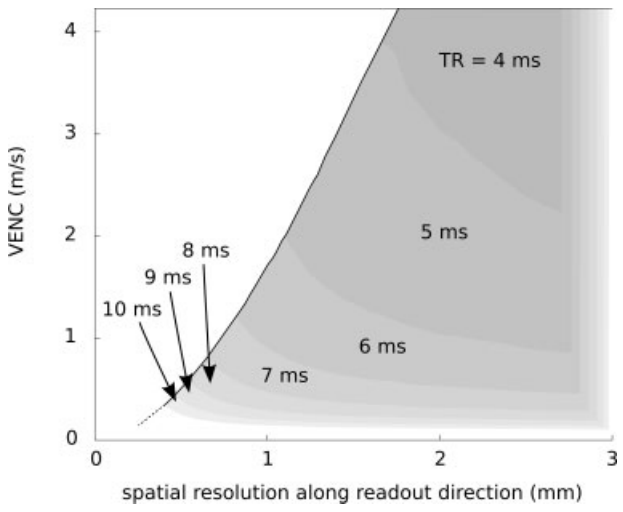


FIG. 5. Trade-offs in three-echo PC-MRI between the spatial resolution along the readout direction, the sequence TR, and the VENC. Each of the partially overlapping shaded regions corresponds to a different TR value. For example, for a 5 ms TR and 1.5 mm spatial resolution, VENC values from 1.3 m/s to 2.8 m/s are possible. Similarly, for a 6 ms TR and a VENC value of 1.5 m/s, spatial resolutions from 1 mm and above are possible. This figure corresponds to a 20 cm FOV.

## CONCLUSIONS

The proposed three-echo sequence allows in-plane velocity-encoding with nearly twice the temporal resolution compared to conventional PC imaging. Measurements obtained using three-echo PC-MRI are in good agreement with conventional PC imaging, and are independent of local resonance offsets.

## REFERENCES

1. Pelc NJ, Herfkens RJ, Shimakawa A, Enzmann DR. Phase-contrast cine magnetic resonance imaging. Magn Reson Q 1991;7:229–254.
2. Pelc NJ, Sommer FG, Li KC, Brosnan TJ, Herfkens RJ, Enzmann DR. Quantitative magnetic resonance flow imaging. Magn Reson Q 1994;10:125–147.
3. Overall WR, Nishimura DG, Hu BS. Fast phase-contrast velocity measurements in the steady state. Magn Reson Med 2002;48:890–898.
4. Markl M, Alley MT, Pelc NJ. Balanced phase-contrast steady-state free precession (PC-SSFP): A novel technique for velocity encoding by gradient inversion. Magn Reson Med 2003;49:945–952.
5. Grinstead J, Sinha S. In-plane velocity encoding with coherent steady-state imaging. Magn Reson Med 2005;54:138–145.
6. Pruessmann KP, Weiger M, Scheidegger MB, Boesiger P. SENSE: Sensitivity encoding for fast MRI. Magn Reson Med 1999;42:952–962.
7. Griswold MA, Jakob PM, Heidemann RM, Nittka M, Jellus V, Wang J, Kiefer B, Haase A. Generalized autocalibrating partially parallel acquisitions (GRAPPA). Magn Reson Med 2002;47:1202–1210.
8. Pai VM, Hecht E, Lee VS, Axel L. High temporal resolution phase contrast MRI using SSFP. In: Proceedings of SCMR, Ninth Annual Scientific Sessions, Miami, 2006.
9. Nielsen JF, Nayak KS. Pulse sequences for phase-contrast SSFP imaging from a single steady-state. In: Proceedings of ISMRM, 14th Annual Meeting, Seattle, 2006. p 879.
10. Nielsen JF, Nayak KS. In-vivo validation of a novel 3-echo SSFP phase-contrast sequence. In: Proceedings of ISMRM Flow and Motion Study Group Workshop, New York, 2006.

11. Bernstein MA, Zhou XJ, Polzin JA, King KF, Ganin A, Pelc NJ, Glover GH. Concomitant gradient terms in phase contrast MR: Analysis and correction. Magn Reson Med 1998;39:300–308.
12. Hargreaves BA, Vasanawala SS, Pauly JM, Nishimura DG. Characterization and reduction of the transient response in steady-state MR imaging. Magn Reson Med 2001;46:149–158.
13. Bernstein MA, Grgic M, Brosnan TJ, Pelc NJ. Reconstructions of phase contrast, phased array multicoil data. Magn Reson Med 1994;32:330–334.
14. Buonocore MH, Gao L. Ghost artifact reduction for echo planar imaging using image phase correction. Magn Reson Med 1997;38:89–100.
15. Chen NK, Wyrwicz AM. Removal of EPI nyquist ghost artifacts with two-dimensional phase correction. Magn Reson Med 2004;51:1247–1253.
16. Schar M, Kozerke S, Fischer SE, Boesiger P. Cardiac SSFP imaging at 3 Tesla. Magn Reson Med 2004;51:799–806.
17. Nayak KS, Hu BS, Hargreaves BA. Wideband SSFP: SSFP imaging with bandwidth greater than 1/TR. In: Proceedings of ISMRM, 13th Annual Meeting, Miami, 2005. p 2389.
18. Griswold MA, Kannengiesser S, Heidemann RM, Wang J, Jakob PM. Field-of-view limitations in parallel imaging. Magn Reson Med 2004;52:1118–1126.